NEBRASKA

Good Life. Great Journey.

DEPARTMENT OF TRANSPORTATION

Early Detection of Near-Surface Void Defects in Concrete Pavement Using Drone Based Thermography and GPR Methods

Final Report

January 2020

UNIVERSITY OF NEBRASKA-LINCOLN

Sponsored by
Nebraska Department of Transportation
Project M082

Disclaimer Notice

This material is based upon work supported by the Federal Highway Administration under SPR-P1(19) M082. The contents of this report reflect the views of the authors, who are responsible for the facts and the accuracy of the information presented herein. The opinions, findings and conclusions expressed in this publication are those of the authors and not necessarily those of the sponsors. This report does not constitute a standard, specification, or regulation.

Technical Report Documentation Page

1. Report No SPR-P1(19) M082	2. Government Accession No.	3. Recipient's Catalog No.	
4. Title and Subtitle Early Detection of Near-Surface Void Defects in Concrete Pavement Using Drone-Based Thermography and GPR Methods		5. Report Date January 31, 2020 6. Performing Organization Code	
7. Author/s Zhigang Shen, Ece Erdogmus, George Morcous, Chongsheng Cheng, Zhexiong Shang, Theresa McCabe, and Anthony Kodsy		8. Performing Organization Report No. 26-1122-0073-001	
9. Performing Organization Name and Address University of Nebraska-Lincoln Durham School of Architectural Engineering and Construction 113 NH, 900 N. 16TH St., Lincoln, NE 68588-0500		10. Work Unit No. (TRAIS)	
		11. Contract or Grant No.	
12. Sponsoring Organization Name and Address Nebraska Department of Transportation 1400 Hwy 2 Lincoln, NE 68509		13. Type of Report and Period Covered	
		14. Sponsoring Agency Code	
15. Supplementary Notes			

16. Abstract

The goal of this research is to evaluate the feasibility and the performance of using UAV-mounted infrared thermography (IRT) and ground penetration radar (GPR) to detect sub-surface voids caused by consolidation issues in concrete pavement. The motivation of the study is to identify the consolidation defects as early as the initial set of concrete to avoid having this problem in large pavement sections, which is costly and time consuming to repair. Using the two technologies in combination to detect subsurface voids in the concrete initial set stage is new and aims to take advantage of the strengths and minimize the limitations of each method. UAV-based IRT can cover large areas of the pavements in a short amount of time, while GPR can provide higher accuracy in locating the defects horizontally and vertically. Therefore, the combination of the two technologies can allow detection of small voids in large areas with improved confidence. In this project, both laboratory and field tests were conducted with both methods, and coring samples were used for validation of results. The results from multiple specimens and multiple experiments suggested that both technologies performed well in detecting the subsurface voids in the concrete pavement's initial set stage. Despite some limitations discussed in the report, the outcomes of the project provided evidence that these technologies can be used separately or together on the field as efficient and economical quality control tools in concrete pavement construction.

17. Key Words Concrete consolidation, early detection, sub-surface voids, thermography, UAV, GPR	18. Distribution Statement		
19. Security Classification (of this report) Unclassified	20. Security Classification (of this page) Unclassified	21. No. Of Pages 33	22. Price

EARLY DETECTION OF NEAR-SURFACE VOID DEFECTS IN CONCRETE PAVEMENT USING DRONE-BASED THERMOGRAPHY AND GPR METHODS

Final Report

January 2020

Principal Investigator
Zhigang Shen

Co-Principal Investigators
Ece Erdogmus, George Morcous

Research Assistants
Antony Kodsy, Chongsheng Cheng, Tess McCabe, and Zhexiong Shang

Authors
Zhigang Shen, Ece Erdogmus, George Morcous, Chongsheng Cheng, Zhexiong Shang, Theresa McCabe, and Anthony Kodsy

Sponsored by
Nebraska Department of Transportation
SPR-P1(19) M082

TABLE OF CONTENT

LIST OF FIGURS

LIST OF TABLES

ACKNOWLEDGEMENTS

This project was sponsored by Nebraska Department of Transportation (NDOT). The research team would like to thank the NDOT Technical Advisory Committee members, especially Ms. Lieska Halsey and Mr. Wallace Heyen. Authors are also greatful for the assistance of UNL's lab manager Peter Hilsabeck, who assisted during slab casting and coring processes.

INTRODUCTION

Poor consolidation in concrete pavement can be costly for highway operation and maintenance. Improper consolidation may cause entrapped air voids beneath the surface of pavement, which after cycles of freeze-thaw, can develop into potholes or spalling. Patching these defects is a costly and time-consuming process, in addition to being inconvenient and dangerous for commuters. Therefore, the early detection of these voids can allow DOTs to identify the problem and fix it before putting the defective sections into service.

Sub-surface (i.e., less than 4 in deep) voids (**Figure 1**) that are 1/2" or larger in diameter (in both horizontal and vertical directions) is a common symptom of consolidation issues during the construction of concrete pavements. This issue was observed by NDOT in concrete pavements constructed by different contractors, on different roads (highways and local roads), and with different thicknesses (9-14 in).

Figure 1 Air void in a cored concrete pavement sample

Although the purpose of consolidation is to reduce the entrapped air from freshly poured concrete, these voids can be caused by improper vibration, overly dry mix, and/or long wait time between concrete batches (Legg 1974). These large voids or concentrations of smaller voids can be detrimental to the durability and/or strength of the pavements (su Jung et al. 2008). The capability of early detection of these voids during the hydration time will allow NDOT field personnel to issue timely correction orders or rework orders to avoid costly repair work after the problematic road section goes in service. The enhanced quality of the concrete pavement will also help to reduce the maintenance cost.

Given the importance of the issue, in this project the investigators experimented two non-destructive evaluation (NDE) methods to detect the subsurface voids during concrete early curing process: the first method is to use infrared thermography (IRT), which utilized the hydration heat generated from the curing process as a background to detect the voids; the second method is to use GPR signals to detect the voids during the curing process. The project outcomes suggested that both methods can successfully detect the defective voids during the early curing time.

In the following sections, experimental methods and outcomes of both investigations using IRT and GPR are reported in detail with limitations noted.

PART 1 : INFRARED THERMOGRAPHIC (IRT) APPROACH

1 BACKGROUND

1.1 Literature Review of Quality Control for Consolidation of Fresh Concrete

Current studies on quality control for fresh concrete consolidation were limited and most of them focused on monitoring the vibration procedure. Although the general practice of consolidation for pavement was recommended by the standard (ACI 309R), the quality control was often relied on the on-site inspectors (Tattersall 2014). The problem with identifying the large voids during the paving is that they were hidden from visual inspection of the finishing surface. Minnich, Mawhorr, & Schipper (1999) developed an accelerometer-based the system to monitor the concrete consolidation based on the vibration rate of the vibrators array. This system provided a real-time display of each vibrator's vibration rate and alarmed the operator when the vibration signal below or above threshold limits. Cable, McDaniel, & Steffes (1999) also reported that through monitoring and controlling the vibration rate, the consistency and the quality of concrete pavement could be improved. A visual monitoring system was developed (Tian et al. 2019; Tian and Bian 2014) to record the position, depth, and duration of vibrator in real-time. This system could assess the vibration effect and visualize the vibration defects to achieve the improvement of quality control during construction. Beside monitoring the status of vibrator, the direct assessment on the fresh concrete was also studied. Alexander & Haskins (1997) developed a device to measure the degree of consolidation through evaluating the change of electrical impedance value during the vibration. It found the curve of AC-resistance against time of vibration was distinguishable for the entrapped air compared to the entrained air and argued the intersection of the two curves to be the indicator of consolidation completion. Although the issue has been well-known among practitioners little effective and practical methods were developed to address it.

1.2 Objective and Scope

The primary goal of this IRT investigation is to develop a reliable and efficient early detection tool for near-surface voids and to enhance NDOT's capacity of quality control during concrete pavement construction. More specifically, the tool is for early detection during the early curing stage, up to 48 hours after the concrete pavement is casted in place. The specific objectives are:

1. To identify the detectability of voids of different sizes and buried depths using temperature contrast
2. To identify best time windows in the first 24 hours after pouring
3. To investigate influences of external factors: curing compound, environmental conditions

2 RESEARCH APPROACHE

2.1 Detection of Near-Surface Voids by Thermography During Hydration

Using thermography to detect sub-face defects in concrete structure has been developed several decades. The typical usage on field is shallow delaminating detection for bridge deck (Abu Dabous et al. 2017; Cheng et al. 2019). It treated the delamination (a horizon crack underneath the deck surface) as an insulator, which blocks the heat flow from the top surface of the deck to the bottom when the sun was heating the deck during the daytime. Thus, the temperature contrast was developed at the deck surface between the delaminated and sound areas.

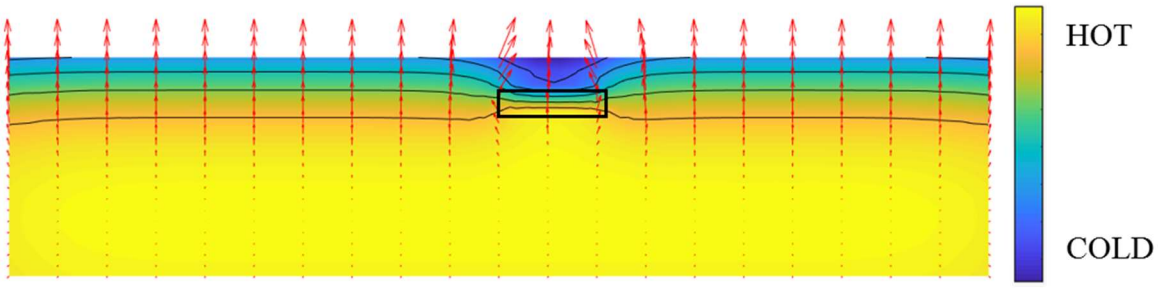

Figure 1.2 Conceptual illustration of detecting mechanism in a section view

This research proposed to detect near-surface void during the pavement construction based on the similar mechanism. The principle for detection is based on the developed temperature contrast of the surface area where the voids are entrapped underneath during the concrete hydration. **Figure 1.2** shows the conceptual illustration of the detection mechanism. It shows the ideal temperature distribution and heat flow for a semi-infinite slab where assumes certain length in depth and infinite length for width. When the poured concrete was setting, the process of hydration continuously generates heat for a certain amount of time (typically tens of hours). When the temperature of concrete is rising quickly and higher than the environment, the temperature inside the slab will be higher in the core location than that closes to surfaces (Jeong and Zollinger 2006; Wang and Dilger 1994). As a result, the heat constantly flows outward from the core of the slab and rapid temperature gradient would occur close to the slab surface (shown as red arrows in **Figure 1.2**). When a larger void or group of small voids occur at the near surface (shown as black box in **Figure 1.2**), they could block the heat flow or/and change the thermal conductivity of the region so that potentially reduce the heat accumulation at the surface of the slab. Thus, presented as the surface temperature, the region having voids underneath could be colder than its surroundings.

3 EXPERIMENTAL DESIGN AND DATA COLLECTION

3.1 Experimental Design for Thermographic Detection

Based on the investigation of thermographic technology and discussions in the technical advisory committee (TAC) meetings, four experiments were designed and conducted. These experiments aim to investigate the applicability of the proposed technology under in-situ conditions for pavement construction. Primarily, the research focus on the detectability of voids in difference sizes and buried depth as well as the best time window during the concrete hydration. In practice, the curing compound will be sprayed (within 10 minutes) after the fresh pavement is consolidated and the surface is finished. Also, the environmental conditions such as ambient temperature and solar heating vary across the day. Thus, this research designed two time-windows for concrete casting (Morning and evening) to investigate the environmental effects.

3.1.1 Apparatus for data collection

This research configured two experimental setups for indoor and outdoor data collections. In the indoor experiments (**Figure 1.3**), the thermal camera was placed on the top of sample slab with downward camera view and record the data continuously. The thermal camera shown in **Figure 1.3c** (FLIR A8300) could provide a 1280x720 spatial resolution with 20 mK sensitivity at 25 ℃. For outdoor experiment, a drone (DJI MATRICE 600) integrated with a thermal camera (FLIR A8300) and on-board camera was hovered over the sample slab for data recording at different time. For both indoor and outdoor experiments, a weather station were used to record the ambient temperature. Also, the thermal coupler (SmartRock) was used to record the concrete internal temperature.

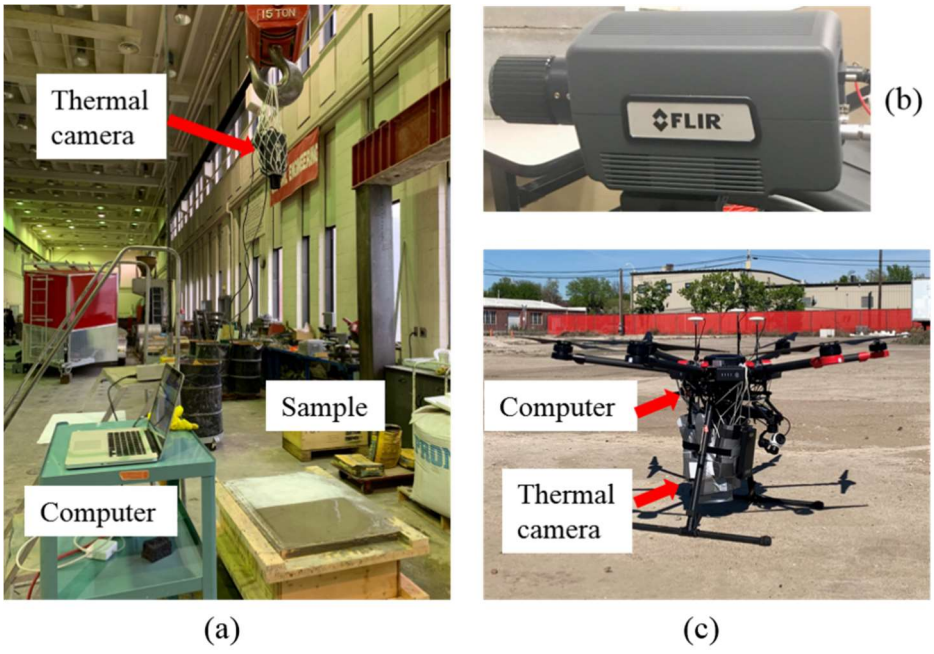

Figure 1.3. Experimental equipment and setups: (a) indoor setup; (b) thermal camera; (c) outdoor setup

Table 1.1 Concretes lab design

Experiment	Dimension (L x W x D)	Mix design	Slump design	Slump tested
EX1(09/28/2018)	32.5"x23"x12"	Quickrete	2.5 in.	N/A
EX2(03/28/2019)	6'x6'x9"	47B	1 in.	0.5 in.
EX3(05/10/2019)	6'x6'x9"	47B	1 in.	2.5 in.
EX4(08/28/2019)	6'x6'x9"	47B	1 in.	1 in.

3.1.2 Evaluation of Effect of Curing Compound (EX1)

The experiment (EX1) was conducted on September 28th, 2018 at the civil structural lab of University of Nebraska-Lincoln. The concrete slab has a dimension of 32.5"x23"x12" in length, width and depth. The concrete mix used was QUIKRETE, a pre-blended mixture, which met the requirements of ASTM C387. The slump test was not conducted at the time of experiment. The artificial voids made with plastic wrapped foam spacing 5 inches were imbedded in 1", 2" and 3" in depth pair-to-pair on the both side of the tape measure shown in **Figure 1.4a**. The curing compound (white pigment cure provided by NDOT) was sprayed on the left half surface of the slab only so that the side-by-side comparison could be observed during the hydration (**Figure 1.4b**). The data was collected up to 72 hours and first 48 hours' data was used for the later analysis.

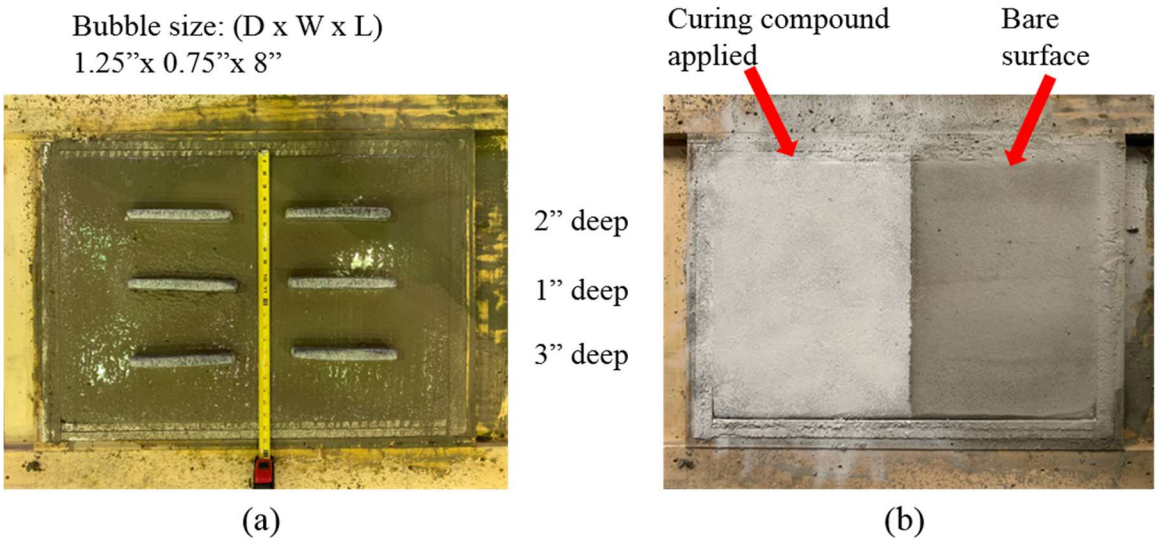

Figure 1.4 Experimental setup for evaluation of effect of curing compound

3.1.3 Evaluation of Detectability and Optimal Time Windows (EX2)

This experiment (EX2) was carried out on March 28th, 2019 at the civil structural lab of University of Nebraska-Lincoln. The concrete slab has the dimension of 72"x72"x9" (length by width by depth). The concrete mix followed 47B mix design with 1 PF cement and 1" slump. The slump of the concrete tested was about 0.5" at the time of experiment. There were four groups of simulated voids imbedded in the slab (**Table 1.1**) to represent small, large, long and air-filled voids in 1", 2",3" and 4" deep. After the concrete was poured, consolidated and surface finished, the artificial voids were deployed followed the layout in **Figure 1.5a** and the thermal coupler was buried in the center location of the slab at depth about 1.5" from surface. **Table 1.2** shows each void's dimension.

Then the surface was re-finished as shown in **Figure 1.5b**. Same white pigment cure (in Section 3.1.2) was sprayed by NDOT professionals after 24 minutes of pour and the surface was shown in **Figure 1.5c**. During time from 3rd hour to 5th hour after pour, the west half part of the concrete slab was covered by a plastic sheet for GPR scanning. The total data for thermal imaging was recorded continuously up to 28 hours.

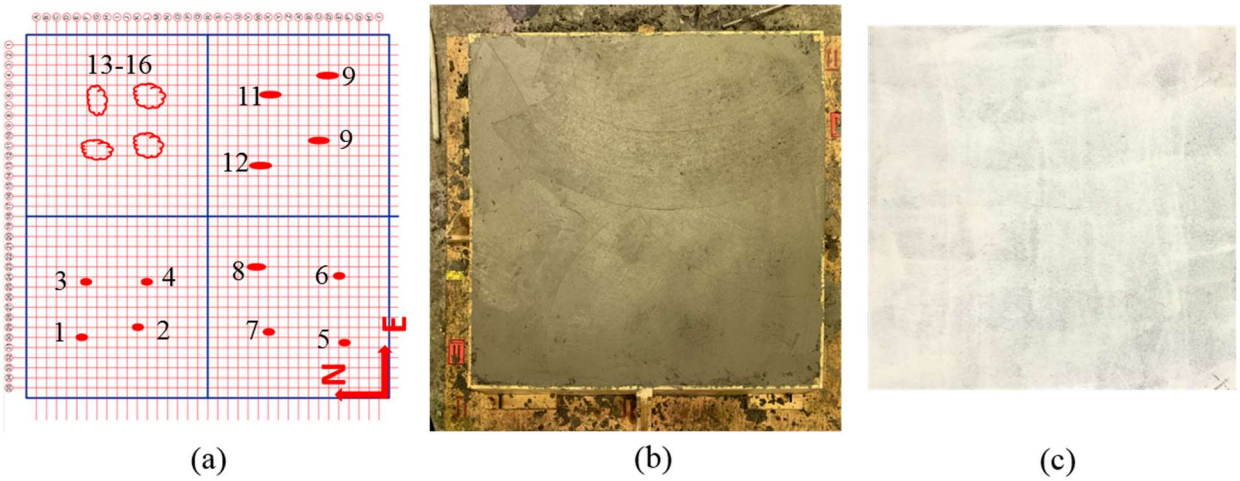

Figure 1.5 Experimental setup for evaluation of detectability and optimal time window

3.1.4 Evaluation of Effect of Outdoor Condition (EX3 & EX4)

There were two experiments conducted at the field closed to the Whitter Research Center of University of Nebraska-Lincoln. Both experiments followed the same form design and same type of artificial voids in Section 3.1.3. The first experiment (EX3) was carried out at 9:10 a.m. on May 10th, 2019 to simulate a morning construction. 16 artificial voids with different sizes were imbedded in the slab after the concrete was consolidated. **Figure 1.6a** shows the location of each void where the distance of void-to-edge and void-to-void was spaced in 12". **Table 1.2** shows the dimension of each void and its corresponding depth. **Figure 1.6b** shows the regular image of the re-finished surface after voids were imbedded before the cure was sprayed. **Figure 1.6b** shows the slab surface after the cure was sprayed. A thermal coupler was placed at the center of the slab (sensor in **Figure.6a**) with depth around 2". The weather station and thermal sensor were continuously collecting the data up to 14 hours. The UAV carried thermal camera collected the data at 9:34 a.m., 9:45 a.m., 10:05 a.m., 11:19 a.m., 12:56 a.m., 2:25 p.m., 3:44 p.m. and 6:25 p.m. The second experiment (EX4) was conducted at 5:30 p.m. on August 28th, 2019 to simulate the evening construction. The form and mix design were shown in **Table 1.1** and the layout, regular image of surface before and after applying curing compound were shown in **Figure 1.6a, b** and **c** accordingly. The weather station recorded the data for 6 hours. The thermal coupler was placed 2" deep. The thermal image was collected at 6:25 p.m., 7:12 p.m., 9:49 p.m. and 11:30 p.m. by the drone.

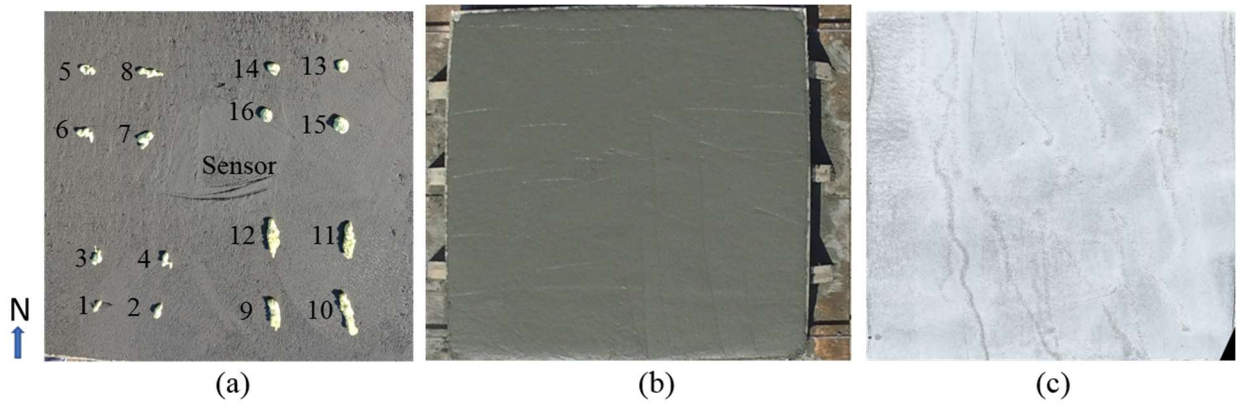

Figure 1.6 Experimental setup for outdoor evaluation of simulated morning construction

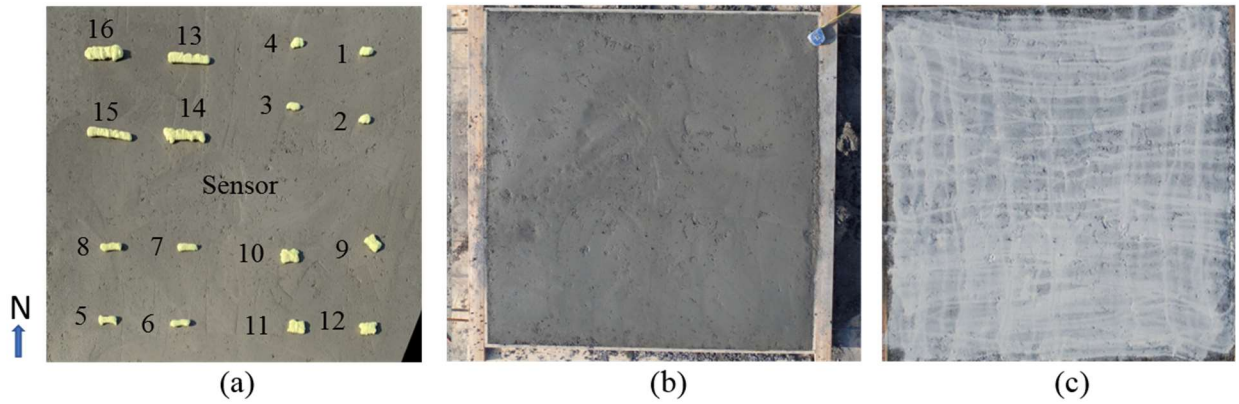

Figure 1.7 Experimental setup for outdoor evaluation of simulated evening construction

Table 1.2 Artificial voids demension and buried depth

	EX2		EX3		EX4	
Void No.	Dimension	Depth	Dimension	Depth	Dimension	Depth
1	2" x 1.5"	-	2" x 0.5"	1"	2" x 1"	1"
2	2" x 1.75"	-	2" x 1"	2"	2" x 1"	2"
3	1.5" x 1.5"	-	2" x 1.5"	3"	2.5" x 1"	3"
4	2" x 1.5"	-	2" x 1"	4"	2" x 1.5"	4"
5	2" x 2"	-	3" x 1.5"	2"	3" x 1"	1"
6	2.5" x 2"	-	3" x 1"	1"	3.5" x 1.5"	2"
7	2.5" x 1.75"	-	3" x 2"	4"	3.5" x 1"	3"
8	4" x 1.5"	-	4" x 1"	3"	3.5" x 1.5"	4"
9	3.75" x 1"	-	5.5" x 2"	1"	2.5" x 2"	1"
10	5" x 1"	-	7" x 2"	2"	3" x 2.5"	2"
11	5.75" x 1"	-	6.5" x 2"	3"	3" x 2.5"	3"
12	6.6" x 1"	-	6" x 2"	4"	3" x 2.5"	4"
13	-	-	2" x 2"	1"	7.5" x 1.5"	1"
14	-	-	2" x 2"	3"	7.5" x 1.5"	2"
15	-	-	3" x 2.5"	2"	7.5" x 1"	3"
16	-	-	2" x 2"	4"	7" x 2"	4"

4 RESULTS

4.1 Results of The Thermographic Analysis

4.1.1 The Effect of Curing Compound

Applying the curing compound has been found two-step influence on the temperature contrast of void defect. First, when the surface was wet (from time window I to II), the temperature contrast (**Figure 1.9** I and II shows the contrast from -0.04 to -0.08℃) was low for both bare surface and surface with sprayed cure. It was found that applying the cure would decrease the temperature at the beginning where in **Figure 1.8** from I to II, the contrast was decreased. This observation was also supported in EX2 (**Figure 1.11)** from I to II that a decrease of temperature contrast was found after applying the cure. Second, when the surface started to dry out, the surface temperature developed quickly. It was shown in **Figure 1.8b** that the surface with sprayed cure increased faster than the bare surface. It could be explained by the function of the curing compound that was designed for water retention. Water evaporation would remove heat from the concrete surface and thus the temperature would be lower at the bare surface than the surface with sprayed cure. As a result, the faster temperature raising at the cure surface developed higher temperature contrast of the void. In **Figure 1.8a III** and **Figure 1.9 III**, the temperature contrast of 1" deep void was around -0.28℃ compared to -0.18℃ of the void at the same depth on the bare surface. At this time stamp, the maximum temperature contrast was reached and started to decrease (**Figure 1.8a IV** and **Figure 1.9 IV**). In summary, applying the cure would decrease the temperature contrast of the void at the beginning while help to develop the contrast later.

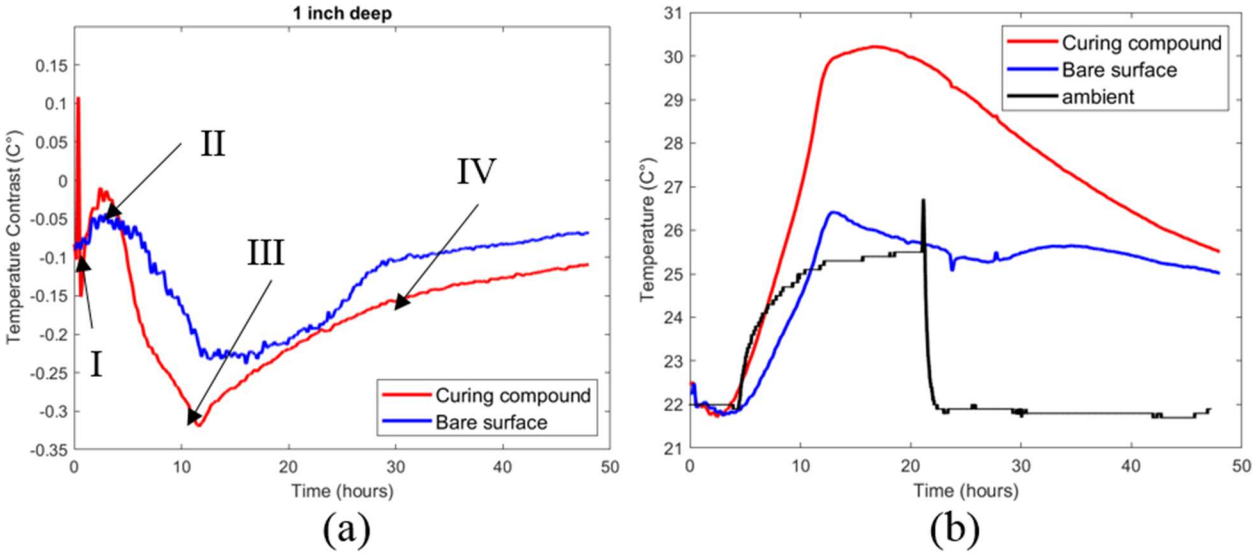

Figure 1.8 temperature evolution after pouring for EX1: (a) temperature contrast for void with 1" depth; (b) temperature for cure sprayed surface, bare surface and ambient temperature

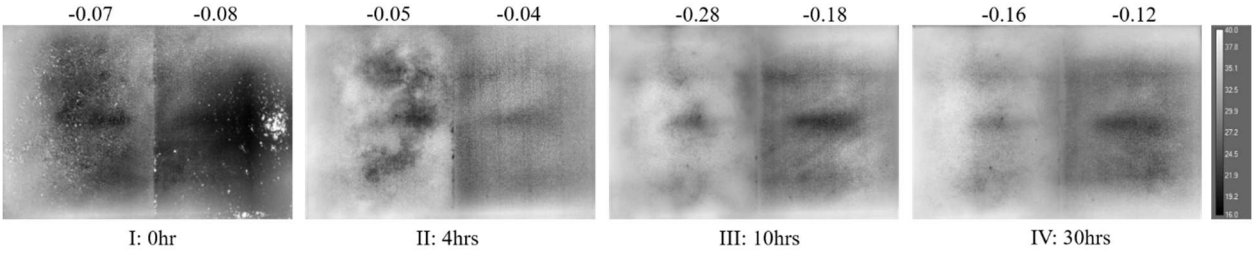

Figure 1.9 Thermal images at different time windows (EX1): left side of each image shows the surface with cure and the right side shows the bare surface

4.1.2 Detectability and Optimal Observation Time Window

The second experiment (EX1) conducted indoor revealed two optimal time windows for potential detection of voids in different sizes and buried depths. The first time-window was observed at the time before cure spray when artificial voids were placed, and the surface was re-finished (**Figure 1.10 I** and **Figure 1.11 I**). At this time window, the voids with small to large shape in depth from 1" to 4" were visible with mean temperature contrast of -0.37°C. This observation was also found in outdoor experiment (EX3) at time **I** in **Figure 1.12** and **Figure 1.13** which a mean temperature contrast of -0.25°C was developed. At time **II**, the curing compound was sprayed, the thermal image in **Figure.11II** shows the decreased visibility of the voids after cure spray. It also clearly shows the sprayed pattern of curing compound. The visibility was further reduced at time **III** where the room temperature (yellow) was higher than the concrete (blue and red in **Figure 1.10**). During time of 3rd hour to 5th hour, the plastic sheet was covered on the top of the slab where the transient thermal behavior for detection was interrupted and interpretation of data was not feasible. Later, at time **IV** and **V** in **Figure 1.10**, the continued temperature raising re-developed the temperature contrast. In **Figure 1.11 IV** and **V**, part of the voids became visible with the temperature contrast of -0.08 (**IV**) and -0.17 (**V**). At time (**Figure 1.10VI** to **VIII**), the temperature raised to the maximum and then started to decrease. In summary, the first time-window could be within the first 20 to 30 minutes before applying the curing compound. The second time-window could be the period of temperature raising after cure spray. However, the factors such as ambient temperature could obstruct the development of temperature contrast which reduce the feasibility of detection.

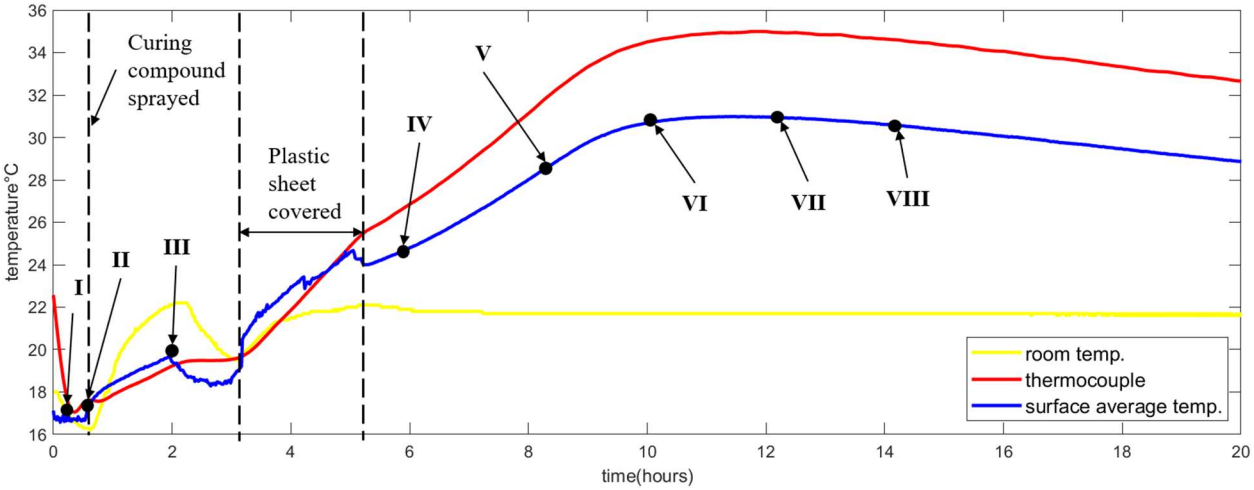

Figure 1.10 Temperature evolution of indoor experiment (EX2)

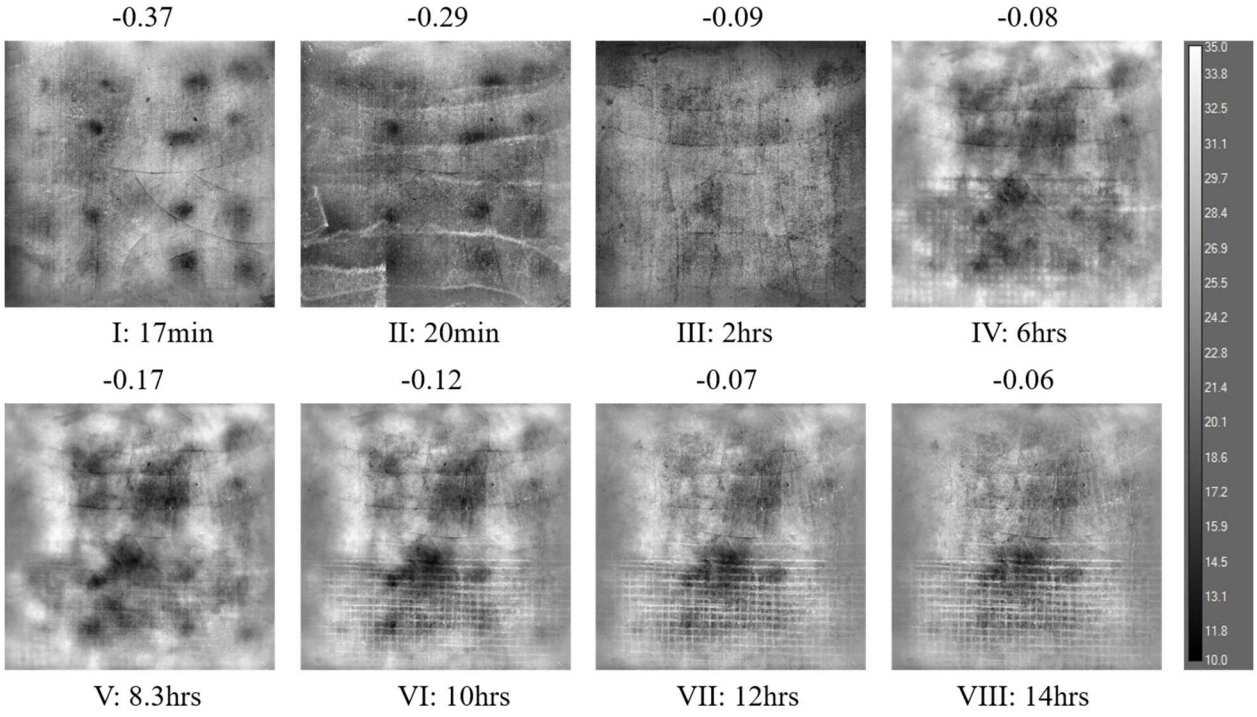

Figure 1.11 Thermal images for indoor experiment (EX2): mean temperature contrast of voids on top; time window on bottom

4.1.3 The Effect of Environmental Condition

Two outdoor experiments (EX3 and EX4) simulating the morning construction and evening construction revealed that the ambient temperature and solar heating were the two major influential factors. Solar heating presented a negative effect on the detectability in **Figure 1.12a**. At the time I in **Figure 1.12a**, the voids were visible with the mean contrast of -0.25℃. After 10 minutes, the contrast was decreased to -0.12℃ and the visibility was low. Later, the voids were no longer observable, and contrast of void even became positive (**Figure 1.13 III** and **IV**) which means the surface temperature above the void was slightly higher than the surrounds. This observation violated the principle of detection and the judgement became confusion. During this period (**Figure 1.12a**), it is found that the mean surface temperature of the slab was close to the thermocouple's reading which was imbedded about 1.5" deep in the slab. According to this period (10 a.m. to 4 p.m. in **Figure 1.12a**), the sun was continuously heating the slab from the top after pouring so that the effect of solar heating could neutralize the heat flow caused by the hydration. At a result, the detectability at this period was low.

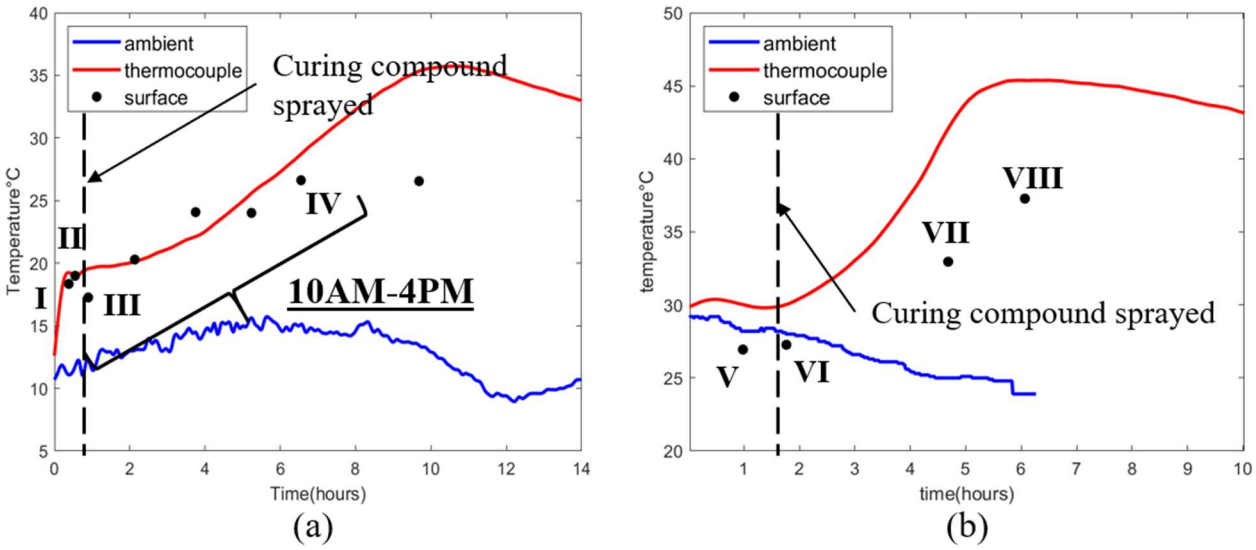

Figure 1.12 Temperature evolution of outdoor experiments: (a) morning construction (EX3); (b) evening construction (EX4)

The ambient temperature is the second factor that affect the detectability through changing the slab's boundary condition for the transient thermal dynamics. It was observed that in the indoor experiment (EX2), when the ambient temperature was higher than the slab's surface temperature, the shallow concrete layer was acutely heated by the ambient through convection. This process was similar to solar heating which would reduce or even inverse the heat flow generated by the hydration. As a result, the temperature contrast developed at the beginning could be reduced to a degree of nontrivial (**Figure 1.10 III** and **Figure 1.11 III**). This effect was also found in the experiment of evening construction (EX4) where in **Figure 1.13 V** and **VI**, the voids having contrast of -0.12 and -0.11℃ and not visual feasible to observe. However, with the development of temperature raising and no solar effect in the nighttime, the temperature contrast of voids increased dramatically (**Figure 1.12**) at time **VII** and **VIII** reaching -0.51 and -0.49℃ (**Figure 1.13**). This observation agreed with two indoor experiments (EX1 and EX2) that during the temperature raising, the contrasts of voids would also increase. This observation could be held true when the ambient temperature was lower than the surface temperature of the concrete slab. In summary, the feasible detection of voids requires the ambient temperature to be lower than the mean temperature of concrete surface.

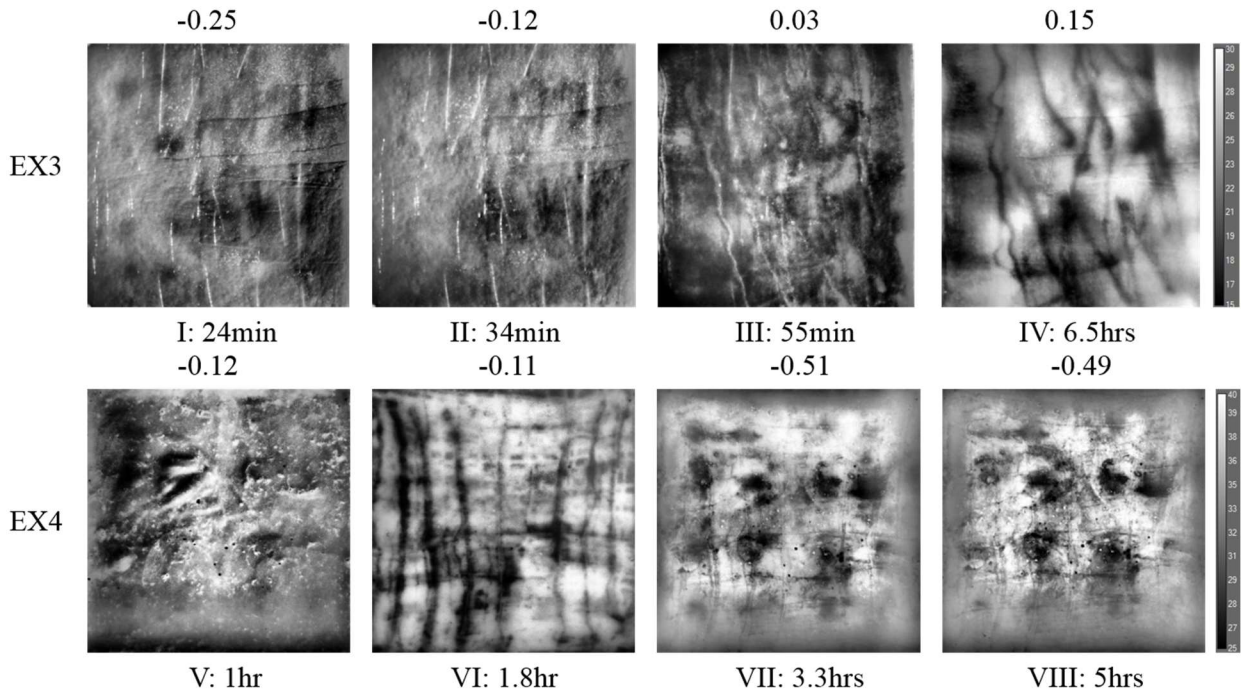

Figure 1.13 Thermal images for different time windows of outdoor experiments

5 CONCLUSION AND RECOMMENDATION

5.1 Conclusions

Based on the four experimental studies (two indoor and two outdoor), applying UAV-based IRT for near-surface voids detection is feasible with favorable environmental conditions. This detectability could be used to qualitatively identify the locations of the concerned voids up to 4" deep. The results of indoor experimentations show that when a temperature contrast is greater than 0.1°C the voids were visually distinguishable given evenly finished concrete surface and uniformly sprayed curing compound. When taking the imperfections of surface finishing and non-uniformity of cure spray into consideration, the voids are visually distinguishable when the temperature contrast was greater than 0.2 ℃ based on the outdoor experiments. Based on the data from the 47B mix design specimen, it took up to 5 minutes for the specimen hydration process to develop the required temperature contrasts.

The curing compound effects on detectability differs depending on the timing of hydration process. At the initial stage of spay, it would decrease the detectability while it is wet. After the compound become a dry film it helps maintaining the temperature contrast for longer time (up to 8 hours given favorable environmental conditions) compared to cases without using curing compound.

The best time window to use the UAV-based IRT for near-surface voids detection without considering the environmental constraints to detect the voids would be within the first 30 minutes after concrete casting and prior to the curing compound application. Furthermore, it was found in this study, after the curing compound application and the heat of hydration heat starts, these two steps will delay voids observation for up to (6-8 hours). The current DOT specification is to start the curing compounds immediately after paving operation but no later than 30 minutes. for paving operations, the UAV-based IRT for near-surface voids detection may not be possible, when the ambient conditions are not favorable.

The favorable environmental conditions required for the UAV-based IRT for near-surface voids detection are the ambient temperature lower than the concrete surface temperature, and no direct solar radiation on the concrete surfaces. Cloudy day, non-rainy and nighttime generally are favorable conditions for near-surface voids detection observation window. Although all experimental setups were quantitatively designed in different sizes and imbed depth, the interpretation of voids' sizes was affected by the external factors including complicated environmental conditions.

5.2 Constrains for Field UAV-IRT surface voids detection

The combination of high-resolution IRT and UAV proved to be a very efficient way to monitor the concrete consolidation quality during pavement time and to detect the subsurface voids in very large concrete pavement areas. However, there are some worth noted UAV constraints in field implementations:

(1) current consumer-grade UAVs' flight control systems can be interrupted or destabilized by strong radio signals presented in the close range. The source of the strong radio signals may come from the communication systems of the construction equipment, concrete delivery trucks, or high-voltage power lines. So, field operators of UAV need to pay close attention and take precaution to identify those potential risks.

(2). If missed the first half-hour observation window, the filed operator will likely have to operate the UAVs after sunset. Currently, FAA requires special permit to fly a UAV in the nighttime, which creates inconvenience for field operations.

(3) In any cases, remote pilot certificate is required to operate in a construction field. It will be the operators' responsibility to make sure the SUVs and the IRT equipment to be insured to avoid liability and property damage issues.

Due to logistical and safety concerns the planned field tests in actual highway project were canceled. Nevertheless, contractors intended to do field implementations need to closely follow the FAA rules of Part 107 Waivers, in addition to the aforementioned constraints.

6 REFERENCE

Abu Dabous, S., Yaghi, S., Alkass, S., and Moselhi, O. (2017). "Concrete bridge deck condition assessment using IR Thermography and Ground Penetrating Radar technologies." *Automation in Construction*.

Alexander, A. M., and Haskins, R. W. (1997). "New field system for measuring degree of consolidation of concrete during vibration." *Transportation Research Record*.

Cable, J. K., McDaniel, L., and Steffes, R. (1999). *Evaluation of Paver Vibrator Frequency Monitoring and Concrete Consolidation*. Iowa State University.

Cheng, C., Shang, Z., and Shen, Z. (2019). "Bridge deck delamination segmentation based on aerial thermography through regularized grayscale morphological reconstruction and gradient statistics." *Infrared Physics and Technology*.

Jeong, J. H., and Zollinger, D. G. (2006). "Finite-element modeling and calibration of temperature prediction of hydrating portland cement concrete pavements." *Journal of Materials in Civil*

Engineering.

Legg, F. E. (1974). *Efficiency of vibrators in consolidating paving concrete*. University of Michigan, Department of Civil Engineering.

Minnich, J. R., Mawhorr, L. R., and Schipper, N. E. (1999). "Accelerometer-based monitoring of concrete consolidation." Google Patents.

Su Jung, Y., Freeman, T. J., and Zollinger, D. G. (2008). *Guidelines for Routine Maintenance of Concrete Pavement*. Texas Transportation Institute, Texas A & M University System.

Tattersall, G. H. (2014). *Workability and Quality Control of Concrete*. *Workability and Quality Control of Concrete*.

Tian, Z., and Bian, C. (2014). "Visual monitoring method on fresh concrete vibration." *KSCE Journal of Civil Engineering*, Springer, 18(2), 398–408.

Tian, Z., Sun, X., Su, W., Li, D., Yang, B., Bian, C., and Wu, J. (2019). "Development of real-time visual monitoring system for vibration effects on fresh concrete." *Automation in Construction*.

Wang, C., and Dilger, W. H. (1994). "Prediction of temperature distribution in hardening concrete." *RILEM Proceedings 25, Thermal Cracking in Concrete at Early Ages*, 21–28.

PART 2: GROUND PENETRATION RADAR (GPR) APPROACH

1 OBJECTIVES

It is proposed here that early detection is possible through the use of GPR, which has been a tool used for roadway quality control since the 1980s (Fernandes and Pais, 2017). The early detection of air voids, however, has been thought to be impossible due to the scattering effects the curing concrete's moisture has on GPR's electromagnetic waves. Thus, this report aims to push the thus-far assumed boundaries of GPR use on concrete structures.

To test the hypothesis of this study, several artificial voids were created using spray insulation foam, a material that has a similar density to naturally occurring air voids, in laboratory slabs. These slabs were then scanned with GPR. Three different slabs of varying sizes and reinforcement were tested with varying void depths and configurations, in order to test the sensitivity of the measurements to void size and depth over time. A typical pavement mix used by Nebraska Department of Transportation (NDOT) was used, namely, 47B Concrete Pavement Mix with 2" (5 cm) slump. Testing was conducted both with and without NDOT's typical curing compound sprayed on top of the slab. GPR scanning began on a 4" x 4" (10 cm x 10 cm) grid, and later transitioned to a 2" x 2" (5 cm x 5 cm) grid for improved accuracy. Scan gridlines were initially stenciled directly onto the top of the slab with chalk. In later stages, a plastic sheet with gridlines was used for ease and repeatability of scanning. Finally, to avoid stripping of the curing compound during early scans, a 4" x 4" (10 cm x 10 cm) plywood sheet was laid out with scan gridlines traced on the top face. Four 1.25" long (3.18 cm) screws were screwed into each corner; this created a stencil with the bottom elevated ½" (1.25 cm) above the surface of the concrete, rather than lying directly on top of it.

2 BRIEF REVIEW OF RELEVANT LITERATURE

Causes of poor consolidation can include insufficient or improper vibration, overly dry mixes, and long wait times between concrete batches. Proper consolidation, therefore, plays a strong role in the hydration of concrete, and its subsequent durability and strength. Therefore, utmost care should be given to proper consolidation during casting. According to Eghtesadi and Nokken (2017), construction defects (such as improper consolidation) are responsible for premature concrete deterioration. They concluded that the effect of insufficient consolidation on concrete durability is more harmful than damage caused by load and thermal effects. However, it should be noted that the level of poor consolidation studied by Eghtesadi and Nokken would rarely be seen in the field. According to Benedetto et. al (2017), one of the areas of main interest for Ground Penetrating Radar (GPR) is its capability to perform accurate, continuous profiles of pavement layers and to detect major causes of structural failure at traffic speed. They state that GPR is one of the most effective and reliable Nondestructive Testing Techniques (NDTs) employed in road surveys due to its high useage flexibility and result reliability. The application of GPR in road engineering relies primarily on impulse radar systems rather than stepped-frequency continuous-wave, due to the relative ease of usage and data interpretation. GPR waves suffer high scattering phenomena due to complex reflection coefficients, similarities between wavelength, and differences between dielectric constants. Clipping of the initial ground wave signal is more common in the case of ground-coupled antennas and causes a particular error in GPR data acquisition.

GPR has been used for roadway evaluation in void detection and rebar cover depth estimation (Al-Qadi, 2003) since the 1980s (Fernandes and Pais, 2017), due to the mobile nature of the process and relative ease of use. Morcous and Erdogmus (2010) also found that metal objects implemented underneath concrete layers improve bottom surface reflectivity and are necessary for a reliable measurement of pavement thickness. They also determined that calibration cores determining the physical dielectric properties of the concrete were essential for accurate calculations of thickness. Liu et al. (2008) compared traditional highway pavement condition detection methods and GPR and found that GPR can provide continuous and nondestructive measurements without disturbing the pavement structure. GPR also has the unique ability to evaluate substructure conditions rapidly, which allows it to be used for the detection of shallow delaminations in continuously reinforced concrete (CRC). High-frequency ground-coupled GPR has been found to work well with concrete pavements for detecting mid-slab-depth delamination and locating steel, or in the identification of possible sub-slab defects such as voids at the interface with the base material. Liu et al. evaluated the capability and effectiveness of the protocol for the detection of early-age delamination in CRC pavements in the field, but unfortunately, they did not quantify “early-age”. Their methods included field tests and coring, numerical analysis, and the collection of other field measurements. Their approach provided improvements in the interpretation of the ground-coupled GPR data and expands the applications of the GPR use.

Another paper that supports the use of GPR for void location was Maierhofer (2003), who explained that GPR is well suited for locating tendon ducts to depths of 50 cm, detecting voids and detachments, locating delamination, and measuring thickness of structures that are only accessible from one side. The limiting condition for concrete thickness determination of elements accessible from only one side is that the maximum thickness that can be measured is 0.5 m using a 500 MHz antenna. The limiting conditions for locating voids and compaction faults in concrete are the size

and depths that can be located with each type of antenna. For instance, voids should be larger than 50 mm and their depth should be less than 0.5 m, with a 500 MHz antenna. Suitable measuring parameters must be defined to guarantee the best resolution and information content of the readings. Maierhofer suggested that another disadvantage to using GPR is when the moisture content is too high, the absorption of the electromagnetic waves increases and there are significant scattering effects. As a result, according to Maierhofer (2003), it is "almost impossible" to investigate fresh and setting concrete with GPR.

Cassidy et al. (2011) compared the performance of both ultrasonic pulse echo and GPR for the detection and location of open voids and steel reinforced concrete sections. GPR is more widely used than ultrasonic pulse echo techniques as it is suitable for a greater range of scenarios. There is limited published research on the practical use of ultrasonic echo-based techniques, particularly when compared to GPR's popularity. GPR has an excellent reputation for being able to detect voids, tendon ducts, and voids beneath concrete sections, but is less successful than ultrasonic methods for the detection of fine voids/fractures within concrete and often requires careful antenna frequency selection and planning. It also requires a skilled operator and expert post-processing.
Shen and Liu (2018) tracked and correlated the relative dielectric constant and hydration process of three concrete specimens: one without admixtures, one with citric acid, and one with triethanolamine. Water plays a strong role in influencing the dielectric properties of concrete, as the dielectric properties depend on the amount and state of the water present. The dielectric properties are comprised of the real dielectric constant, which is represented by the relative dielectric constant (RDC) and an imaginary part related to dielectric losses. The variations of concrete phases during curing lead to shifts in RDC. Because the dielectric loss depends on conductivity loss and the dielectric polarization loss, it is determined, for the most part, by the concrete's electrical conductivity and RDC. The early hydration process of concrete can be also divided into four stages: the dissolution period (0-60 minutes), the setting period (60-340 minutes), initial hardening (340-450 minutes), and the hardening period (after 450 minutes). Shen and Liu found that GPR amplitude and RDC are the most reliable ways to understand how the concrete's microstructure and hydration will develop within the first 72 hours. They also found that the dielectric properties can accurately determine the hydration process and final setting of concrete in the first 72 hours.

In another case study, Li et al. (2016) compared GPR and stress-wave techniques to assess the condition of concrete pavements. A jointed concrete pavement segment with potential air voids between the concrete and granular layers was monitored to understand the differences between the NDE methods that have been used successfully by different researchers and transportation agencies to detect large voids under rigid pavement. The authors noted that moisture content, concrete consolidation, presence of highly conductive material, and size of the defect could affect the reliability of GPR results. The moisture content of the material can significantly affect its dielectric constant value, as the dielectric constant value of a high moisture content material is significantly higher than that of the same material in dry conditions. The GPR data on the experimental segment was acquired by a single cart-mounted high frequency (1.5GHz) ground coupled antenna. The raw GPR data was processed with an assumed dielectric constant for dry concrete to convert reflection times to depths. The obtained average dynamic modulus of concrete was more consistent and reliable than the average dynamic modulus calculated based on the full wavelength range, as the influence of the under-layer material and air voids identified between

their interface were excluded. Relatively low dynamic modulus values were identified at the base of the concrete layer, which was an indication of potential air voids between the concrete and granular base layers. Reversed polarity of GPR signals at the interface between the concrete and granular base layers indicated air voids, because the velocity of the electromagnetic waves increases when they propagate into an air void. Air voids were identified and measured 0.5" (1.27 cm) from the bottom of core locations, which supported the data taken by GPR. As a result, Li et al. concluded that GPR proved to be an accurate method to estimate the thickness of concrete pavement in this study. Air voids at the concrete-granular base interface were characterized by the reversed polarity of GPR signals and confirmed by core samples in nearby locations. This information is especially relevant because voids are highly likely during poor consolidation both in concrete and between the concrete and granular layers. GPR being validated as an accurate method to estimate the thickness of pavement by Li et al. provides support for the aims of the current study with respect to detecting of air voids.

3 LAB EXPERIMENTS

Three slabs were tested in the structures laboratories of University of Nebraska-Lincoln (UNL). The first slab tested was a 48" x 48" x 7.5" (1.22m x 1.22m x 19 cm) and reinforced with four #4 bars spaced at 12" as shown in **Figure 2.1**. The bars in the x-direction had a depth of 5.5" (13.9 cm), and the bars in the y-direction were at a depth of 6" (15.2 cm). It included small artificial air voids varying in dimensions from 0.5" – 1.5" (1.27cm – 3.81cm) and they were embedded at depths of 0.5", 1", 1.25", 2", and 3" (1.27 cm, 2.54 cm, 3.16 cm, 5.08 cm, 7.62 cm) as shown in **Figure 2.2**. GPR detection tests were conducted one week after the specimen was poured in this first trial, and line scans were done at 4" (10 cm) spacing.

Figure 2.1 Slab 1- Specimen Photo and Scanning Axes

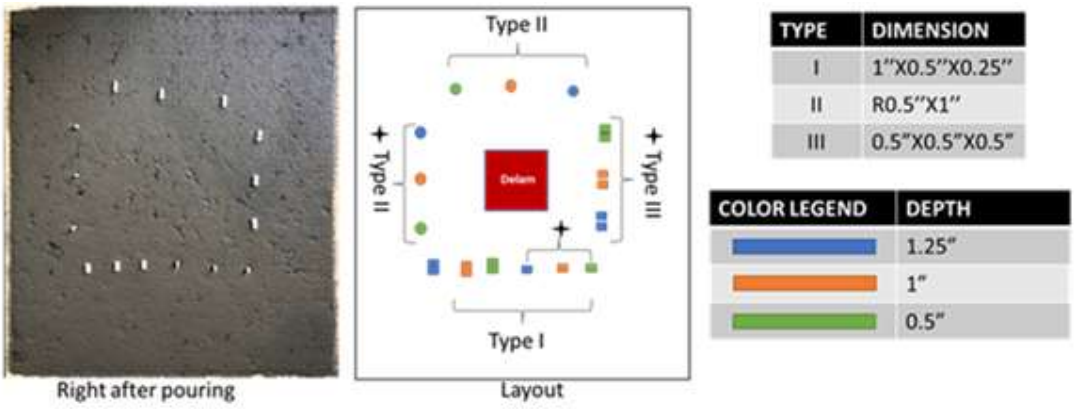

Figure 2.2 Slab 1 - Void Plan View

GPR was able to detect the reinforcement and two unidentified anomalies at a depth of 5", assuming a dielectric constant of 6.25. It was not possible to detect the smaller voids (**Figure 2.3** and **Figure 2.4**).

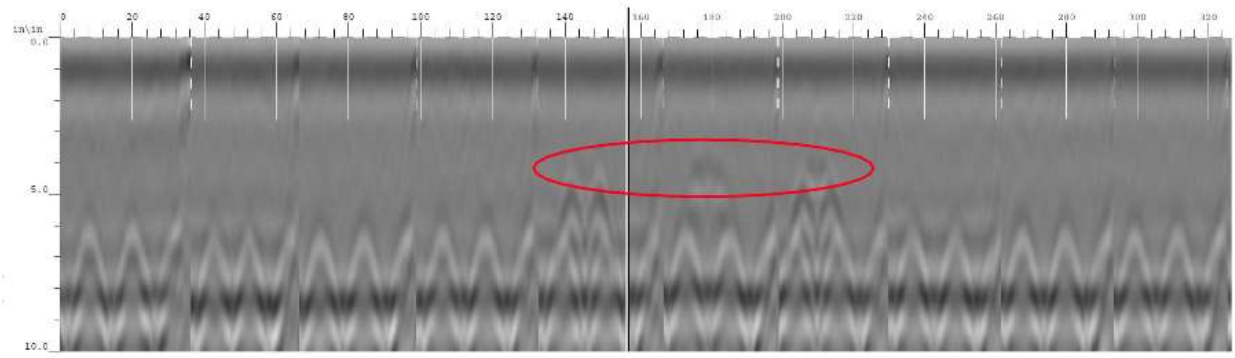

Figure 2.3 Slab 1 - Continuous Scans in the X-Direction

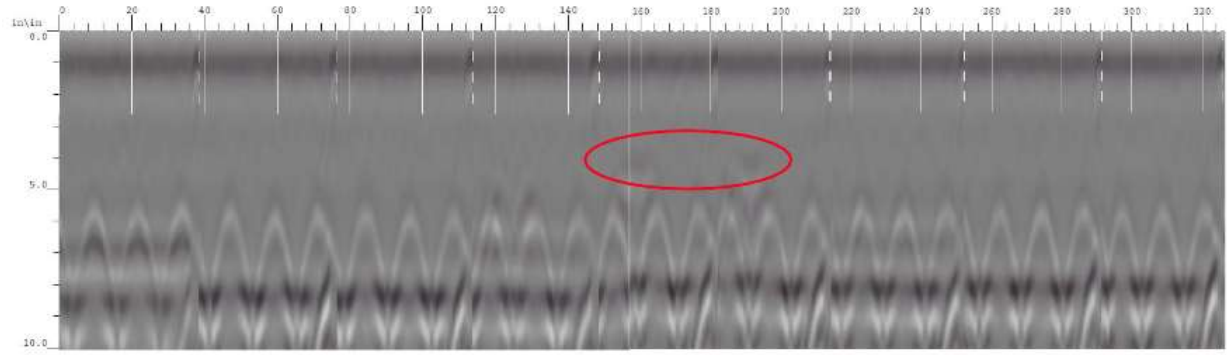

Figure 2.4 Slab 1 - Continuous Scans in the Y-Direction

After this experiement, it was decided to use air voids with dimensions larger than 1.25" (3.16 cm). Based on the experience of NDOT pavement engineers, voids of this size and larger can have detrimental effects on the pavement durability, while those smaller can be neglected.

A second slab measuring 44” x 40” x 8” (1.12m x 1.02m x 0.20m) was cast. This specimen was reinforced with two #4 bars placed 1.5” (0.04m) from the slab end in both directions at an average depth of 6.25” (0.16m) in order to give the slab enough strength to move it around in the lab if needed, without major damage. This slab used two cubic yards (1.53 m^3) of NDOT 47B Concrete Pavement Mix with 2” (0.05m) slump. Insulation spray foam was used to create the voids (**Figure 2.5**), which were implanted after the slab was divided into four quadrants in order to group the different void sizes and depths (**Table 2.3**) in each quadrant (**Figure 2.5, Figure 2.6**).

Figure 2.5 Slab 2 – Small Artificial Air Void

Table 2.3: Slab 2 - Void Dimensions

Void Size Category	**Large Voids**			**Small Voids**		
Void Number	4	5	6	7	8	9
Dimensions	2” x 1.75” (5.08cm x 4.45cm)	2” x 1.5” (5.08cm x 3.81cm)	1.5” x 1.5” (3.81cm x 3.81cm)	1.75” x 0.75” (4.45cm x 0.91cm)	1.25” x 1.25” (3.18cm x 3.18cm)	0.75” x 1.5” (0.91cm x 3.81cm)
Depth	2” (5.08cm)	2” (5.08cm)	2” (5.08cm)	1” (2.54cm)	1” (2.54cm)	1” (2.54cm)

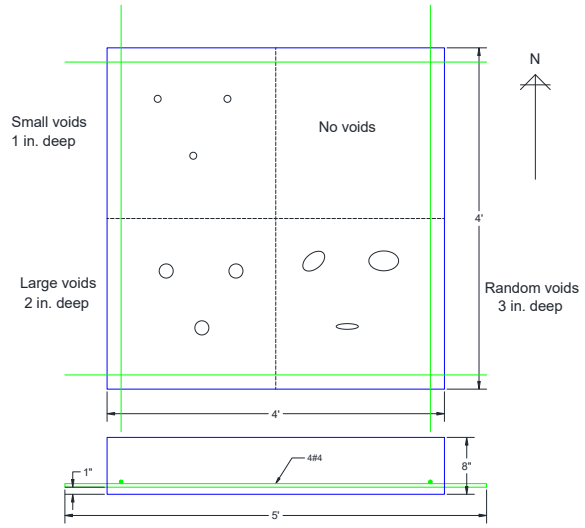

Figure 2.6 Slab 2 - Void Types and Depths with Rebar Locations

Random voids shown in the bottom-right corner of **Figure 2.6** were created by directly injecting the insulation spray foam into the concrete, so that the artificial voids' sizes and shapes were unknown. One quadrant (top right in **Figure 2.6**) was left without any voids to function as the control quadrant. The concrete was consolidated using internal vibration, and then the surface was finished and covered with a plastic sheet for curing. No curing compound was used on this specimen.

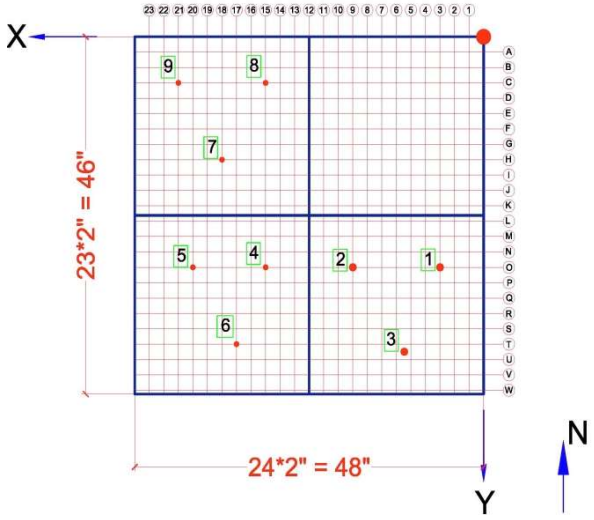

Figure 2.7 Slab 2 – Core Numbers and GPR grid lines

The slab was scanned with GPR at 5 hours and 24 hours, as well as 2, 4, and 9 days after pouring. GPR line scans were initially done at 4" (0.10m) o.c., and later the slab was scanned at 2" (0.05m) o.c. in both directions (**Figures 2.7**, **2.8, and 2.9**).

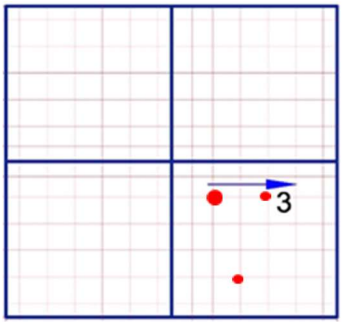

Figure 2.8 Slab 2 –Illustration of the Five Hour Scan of Southeast Corner with Void Locations and Scan Direction

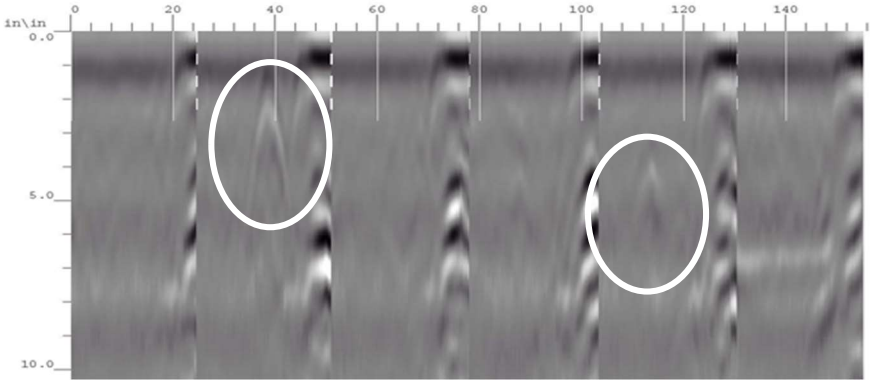

Figure 2.9 Slab 2 - Five Hour Scan of Southeast Corner

After all scanning is completed, core samples were taken at locations where strong signals for anomalies were detected. **Figure 2.10** shows examples of signals with different strengths.

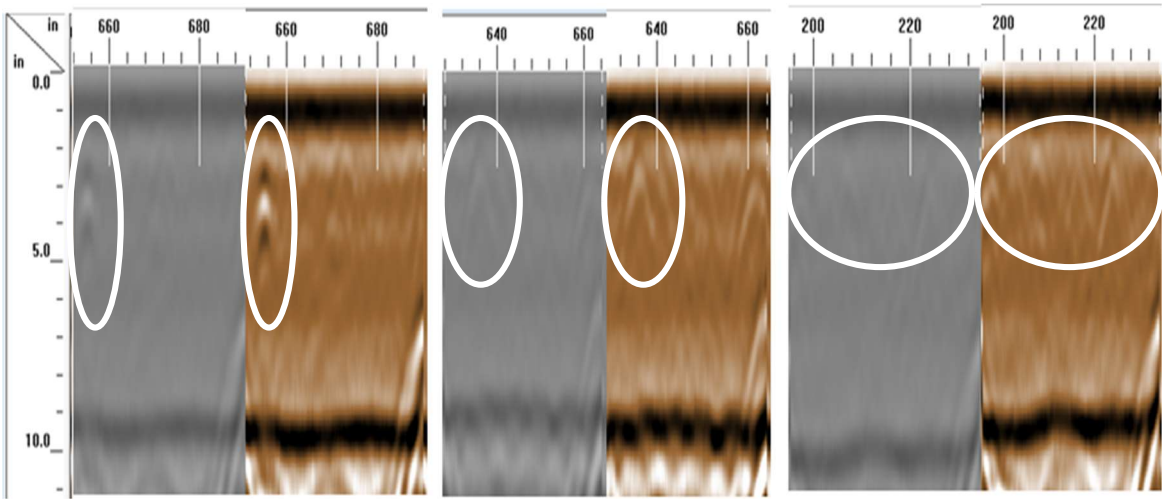

Figure 2.10 From Left to Right: Clear, Mid, and Vague Signal Examples Using Default Setting and Post Processing

After nine days, the slab was cored in 10 places based on the void locations detected by GPR. The results of the GPR scans as validated by the inspections of the cores are shown in **Table 2.4**. At least one of each type of void was successfully located in the cores. In addition to the nine cores taken in each of the three quadrants with artificial voids, Core 10 was taken from the control quadrant. GPR signals picked up very fine air signals throughout this cross section, even though

there were no artificial voids located there. As expected, these were fine air bubbles of negligible size that formed naturally during consolidation. This laboratory experiment helped to determine the lower size limit – 1.5 inches – of air voids that could be detected in the top four inches of pavement.

Table 2.4: Slab 2 - Void Coring Results

Core Number	Embedded Voids	GPR Signal clarity	Coring Results	Notes
1	Large Free Spray	Clear	Visible artificial void	
2		Clear and Vague	No artificial void at center	Void located half a core diameter off Other, smaller voids present at location of vague signal
3		Clear	Visible artificial void	
4	Large Pre-Sprayed and Hardened Foams	Vague	No artificial void	Void located half a core diameter off Other, smaller voids also present
5		Clear	Visible artificial void	Fine voids also present
6		Clear	No artificial void	No void present when coring
7	Small Pre-Sprayed and Hardened Foam	Vague	No artificial void	No void present when coring Fine voids present
8		Clear	No artificial void	No void present when coring Questionable location
9		Clear	Visible artificial void	
10	No Voids	Moderate	No artificial void	Fine voids present

A third slab measuring 72"' x 72" x 9" (1.83m x 1.83m x 0.23m) was cast in UNL's structural lab using NDOT 47B concrete. Two types of artificial voids were created in the slab at depths of 1" - 4" (0.025m – 0.10m). Type One voids were created by using insulation spray foam – the same foam successfully used in Slab 2. Type Two voids were created by injecting compressed air directly into the concrete slab to form the random voids. The voids' locations were measured from the southwest corner of the slab (the "origin") and are recorded as shown in **Table 2.3**.

Table 2.5: Slab 3 - Void Dimensions and Locations

Core No.	Void Size (Quadrant)	Void Dimension	Location from origin (Inches), (Meters)
1	Type One: Small (NW Corner)	2" x 1.5" (0.05m x 0.038m)	(12, 59), (0.3, 1.5)
2		2" x 1.75" (0.05m x 0.04m)	(14, 50), (0.4, 1.3)
3		1.5" x 1.5" (0.038m x 0.038m)	(23, 60), (0.6, 1.5)
4		2" x 1.5" (0.05m x 0.038m)	(23, 48), (0.6, 1.2)
5	Type One: Large (SW Corner)	2" x 2" (0.05 x 0.05m)	(11, 9), (0.3, 0.2)
6		2.5" x 2" (0.06m x 0.05m)	(26, 10), (0.7, 0.3)
7		2.5" x 1.75" (0.06m x 0.04m)	(13, 24), (0.3, 0.6)
8		4" x 1.5" (0.10m x 0.038m)	(26, 26), (0.7, 0.7)
9	Type One: Long	3.75" x 1" (0.095m x 0.03m)	(64, 12), (1.6, 0.3)
10		5" x 1" (0.13m x 0.03m)	(51, 13), (1.3, 0.4)

11	(SE Corner)	5.75" x 1" (0.15m x 0.03m)	(60, 23), (1.5, 0.6)
12		6.5" x 1" (0.17m x 0.03m)	(46, 26), (1.2, 0.7)
13-16	Type Two: Compressed Air (NE Corner)	Random	Unknown

NDOT's Right Pointe White Water Wax concrete curing compound was sprayed on the top surface to follow typical field processes. NDOT routinely sprays this particular curing compound right after concrete placement. When GPR is used on wet curing compound, the wheels of the handheld GPR removes lines of compound, likely reducing its effectiveness (**Figure 2.11**). GPR scanning was conducted on a 2" x 2" o.c. grid (0.05m x 0.05m) on the western half of the slab, 3 hours and 4 hours after pouring, and on the entire slab 24 hours after pouring. **Figure 2.12** illustrates the slab with cardinal directions and void locations, as well as the location of the linear scan, results of which are presented in **Figure 2.13-15**.

Figure 2.11 Slab 3 – Image after Scanning the Slab with GPR at 3 and 4 Hours on Curing Compound

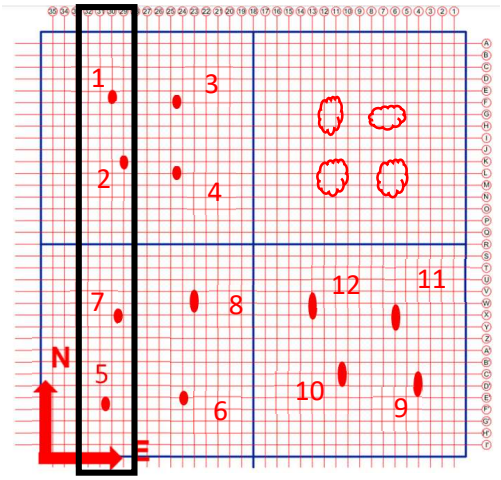

Figure 2.12 Slab 3 – North-South Linear Scan Location (denoted by rectangle) at 3, 4, and 24 Hours. Corresponding scans are presented in Figures 2.13, 2.14, and 2.15, respectively.

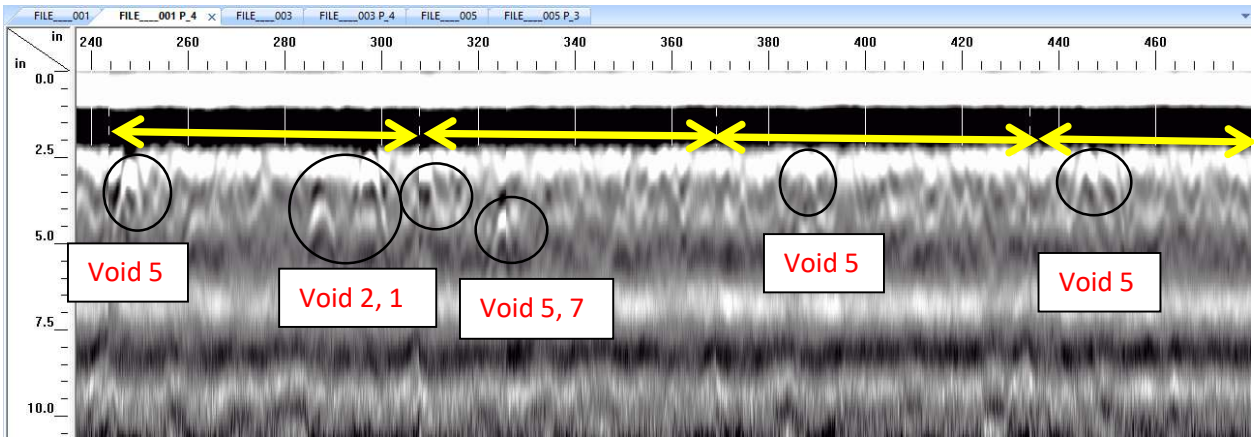

Figure 2.13 Slab 3 - North-South Scan at 3 Hours

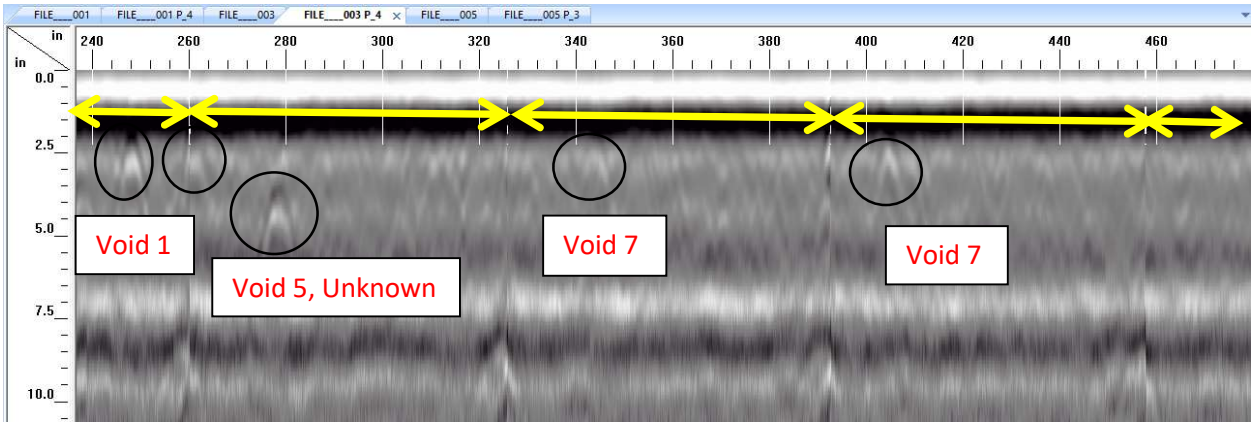

Figure 2.14 Slab 3 – North-South Scan at 4 Hours

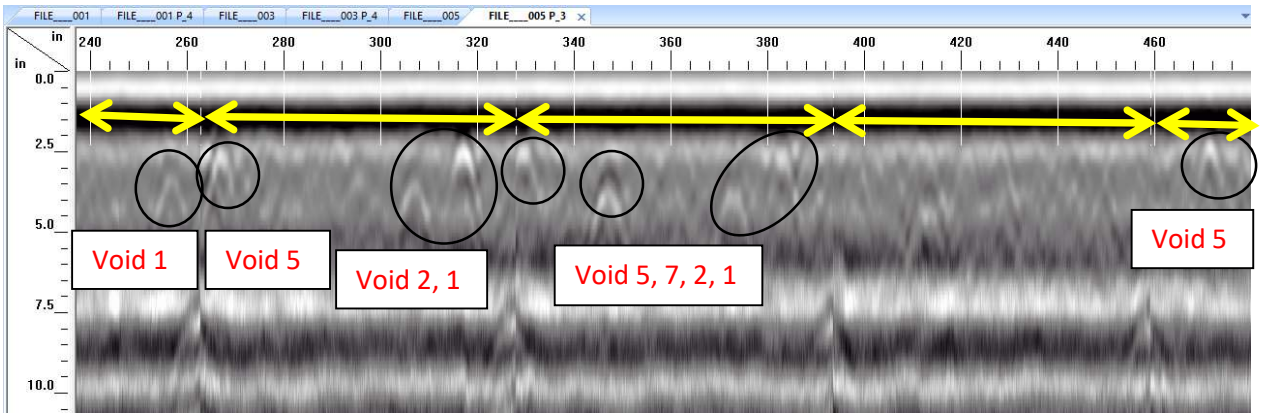

Figure 2.15 Slab 3 - North-South Scan at 24 Hours

Due to lab space restrictions, the slab was moved outside after the GPR testing, and coring was completed while it was outdoors. Only three verification cores were taken out of the 16 void locations, due to a combination of time constraints and inclement weather during coring (**Figures 2.17-2.19**). Cores were taken at void locations 8, 12, and 13; to test for the detection of large voids, oblong voids, and compressed air, respectively. No cores were taken for small voids (1-4), since these smaller size voids (around 1" x 1") had been successfully detected and cored in previous

testing. Core 8's GPR scans showed one of the weaker signals, whereas Core 12's GPR scan was one of the strongest signals. This can be explained by the surface area perpendicular to the direction of the magnetic waves. It is naturally easier to detect the oblong void parallel to the surface (**Figure 2.18**) compared to detecting a smaller are (**Figure 2.17**). The signals for the compressed air area were vague but a core was taken anyway to see the effects of the inserted compressed air. It appeared that the compressed air was dispersed into fine bubbles as the concrete consolidated, which explains the vague signals (**Figure 2.19**).

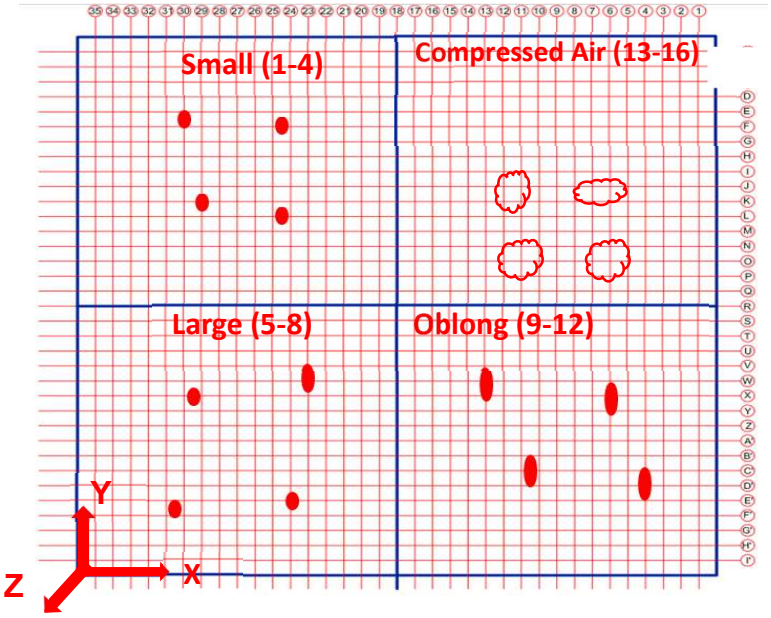

Figure 2.16 Slab 3 - Void Location and Scanning Coordinate System

Figure 2.17 Slab 3 - Core 8 (Large Void)

Figure 2.18 Slab 3 - Core 12 (Oblong Void)

Figure 2.19 Slab 3 - Core 13 (Compressed Air)

Table 2.4 shows the average percent error and average inches off between the assumed physical locations (measured as the anomalies are inserted into wet concrete) and the GPR detected locations for Slab 3. It is important to note that the 3 and 4 hour scans' average percent error and average inches off did not take into account voids 9 – 12, as only the western half of the slab was scanned at 3 and 4 hours. The 24 hour scan results shown in **Table 2.4** include voids 9 – 12.

As is evident from **Table 2.6**, the percent error is less than 3% for the x and y-directions on the coordinate system, with the exception of the four hour-scan in the y-direction. The larger error (10.8%) can be explained by the slight shift in the starting point of the scan each time, since a removable stencil was used. This minor variation is also evident in the scans shown in **Figures 2.13-15**. Therefore, if several readings are to be taken for repeatability and the validaton of data, care must be taken to ensure the start of the scan line is kept consistent. This presents an advantage of marking the gridlines directly on the surface instead of using a stencil, even though it would add significant time to the process if several measurements are to be taken over a long pavement section. The compromise is to place physical marks on the surface for the starting lines in each direction and align the stencil over these lines at each reading, but this would only be possible after the curing compound is dry. Despite these errors, the average number of "inches off" between the GPR-based location and the assumed location is only 1.5" or less (excluding the reading at four

hours in the y-direction), which is less than half of a coring cylinder's diameter (4"). Meanwhile, for the outlier reading of four hours in the y-direction, the average number of "inches off" is only 0.5" outside of the coring diameter. The z-direction (depth) scans seems to give the largest error in percentage, however, in dimensions, the error is not as high. The additional error in the measurement of depth also relates to the fact that depth readings will be most affected from the changing dielectric constant as concrete cures and a concrete test slab sitting on concrete lab floor makes it difficult to adequately determine the base of the test slab for dielectric constant calibration. However, the researchers or NDOT engineers were not concerned with the z-direction errors, since it is more crucial to locate these voids horizontally than vertically.

Table 2.6: Slab 3 - Average Percent Error Hourly Comparison

Coordinate Direction	**X**			**Y**			**Z**		
Time Scanned	3 Hours	4 Hours	24 Hours	3 Hours	4 Hours	24 Hours	3 Hours	4 Hours	24 Hours
Avg Percent Error (%)	-2.9%	-0.7%	-2.4%	-1.6%	-10.8%	1.6%	44.8%	35.4%	26.4%
Avg Inches off	1.5"	0.75"	1.25"	1.25	2.5"	0.75"	1"	0.5"	0.7"

Table 2.7 compares the assumed location of the artificial void to its GPR based location for Cores 8 and 12 (**Figure 2.17** and **Figure 2.18**). Since the cores were taken centering the GPR detected locations, the center of each core corresponds to the GPR detected location. As can be seen the error is between 0.5" and 1" for these cores.

Table 2.7: Slab 3 – Cores 8 and 12 Assumed vs. GPR Detected Location

Core Identifier	**Core 8**	**Core 12**
Assumed Location	4"	4"
GPR Detected Location	3.5"	3"
Inches off	0.5"	1"
Signal Strength	Weak	Strong

4 FIELD EXPERIMENTS

The initial field experiment (Field Experiment 1) was conducted in late September, 2017. A 4' x 4' (1.22m x 1.22m) section of pavement on I-80 Eastbound between milepost 430.6 and 438.8 was scanned at 4" (0.10m) o.c. for void detection. NDOT pavement engineers have previously determined that yellow staining on the surface of aged concrete pavements were indicators of consolidation voids. Therefore the scanning grid was set up based on these stains on this stretch of highway.

Figure 2.20 and **Figure 2.21** show an illustration and a photo of the scanning grid, respectively. **Figure 2.22** shows the resulting scans and detected voids, with the circles corresponding by color to those on 21.

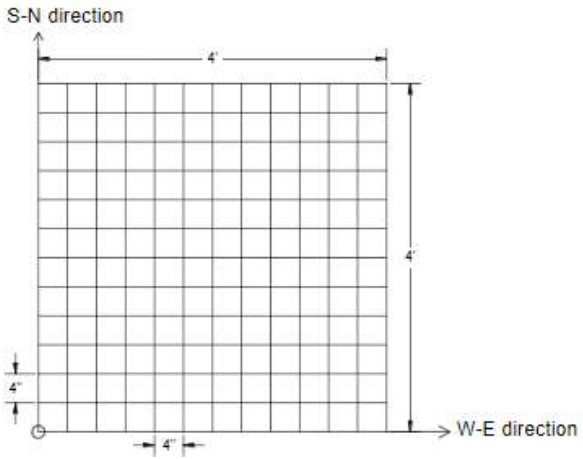

Figure 2.20 Field Experiment 1 - Scanning Grid

Figure 2.21 Field Experiment 1 - Scanning Grid with Suspected/Detected Voids

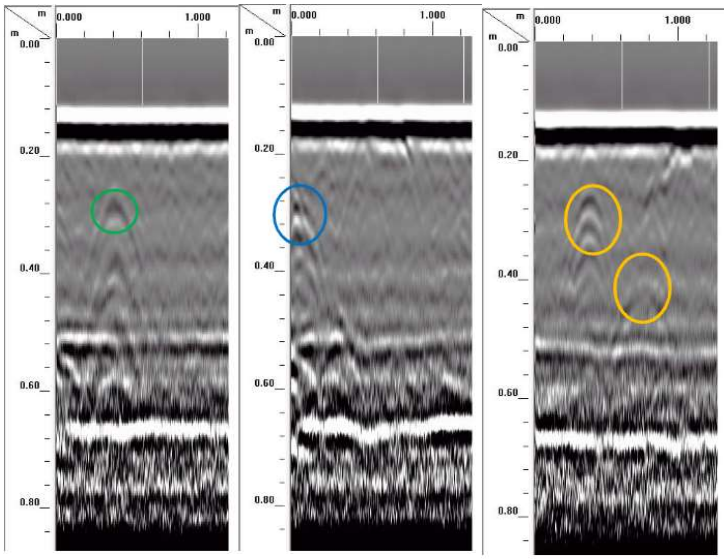

Figure 2.22 From Left to Right: 1st and 10th Scan Lines in the W-E Direction, 6th Line in the S-N Direction

In conclusion, the void locations were correlated to the yellow spots on the pavement surface, and this could be verified with GPR. In this case, the concrete tested was not fresh.

The second field experiment was conducted in late October 2019 where the high temperature was 57°F on a section of pavement on Highway 30, west of North Bend, NE. This pavement was cast 6 weeks prior to scanning. A 4' x 4' x ¾" (1.22m x 1.22m x 1.9 cm) sheet of plywood with screws on the four corners (to elevate it ½" above the concrete) was laid on the pavement, and the GPR scans were conducted on a 4" x 4" (0.10m x 0.10m) o.c. grid (**Figure 2.23**). The 4" x 4" (0.10m x 0.10m) grid was marked on the plywood sheet for ease of use. Scans were not done on a 2" x 2" grid, as the team wanted to scan as many different spots as possible and it was faster to scan at 4" x 4" o.c. GPR scans did not pick up any voids in the top four inches of the pavement , which is the depth NDOT was most interested in; and coring at each scanning location yielded no voids (of a size of concern) in that region as well (**Figures 2.24-2.26**). The researchers concluded that there was proper consolidation at this location and the experiment was successful.

Figure 2.23 Field Experiment 2 - GPR Scanning

Figure 2.24 Field Experiment 2 - Core 1

Figure 2.25 Field Experiment 2 - Core 2

Figure 2.26 Field Experiment 2 - Core 3

5 CONCLUSIONS

Based on the experimental investigations, it was concluded that GPR can detect air voids (honeycombing) ranging in size from 1.5” (3.8 cm) to 4” (10 cm) in concrete pavement as early as three hours after concrete placement. Scanning at 2” (5 cm) spacing is recommended for the better detection accuracy. However, scanning at 4” (10 cm) spacing still provide acceptable detection accuracy and saves scanning time. Voids as small as 1.5” (3.81 cm) in diameter are detectable with GPR if located in the top 4” (10 cm) of concrete pavement, which is more critical to pavement durability than deeper voids. To avoid damaging the curing compound sprayed on the top of concrete pavement, a stencil made of plywood can be used elevated above the concrete with no

contact to the pavement surface. With such a solution, GPR scanning and detection of air voids as early as three hours is possible with an error margin of less than 3% or 1.5 inches at most, as verified by concrete cores. Larger errors are possible, if a stencil is used for gridlines and the start line of scans shift slightly from the intended origin at a particular reading, as was the case for the 4 hour scan in the y-direction for Slab 3. Overall, it is concluded that with carefully laid scan grids and post-processing, GPR can be a powerful NDT method for the early detection (as early as 3 hours from casting) of honeycombing in concrete pavements.

6 REFERENCES

Al-Qadi, I., Lahouar, S., & Loulizi, A. (2003). Successful Application of Ground-Penetrating Radar for Quality Assurance-Quality Control of New Pavements. *Transportation Research Record: Journal of the Transportation Research Board,1861*, 86-97. doi:10.3141/1861-10

Benedetto, A., Tosti, F., Ciampoli, L. B., & D'Amico, F. (2017). An overview of ground-penetrating radar signal processing techniques for road inspections. *Signal Processing,132*, 201-209. doi:10.1016/j.sigpro.2016.05.016

Cassidy, N. J., Eddies, R., & Dods, S. (2011). Void detection beneath reinforced concrete sections: The practical application of ground-penetrating radar and ultrasonic techniques. *Journal of Applied Geophysics,74*(4), 263-276.

Eghtesadi, S., & Nokken, M. (2017). Effect of Cracking and Improper Consolidation as Important Concrete Defects on Water Absorption and Electrical Conductivity. *Journal of Materials in Civil Engineering,29*(11), 04017201. doi:10.1061/(asce)mt.1943-5533.0002050

Fernandes, Francisco M., and Jorge C. Pais. "Laboratory Observation of Cracks in Road Pavements with GPR." *Construction and Building Materials*, vol. 154, 2017, pp. 1130–1138., doi:10.1016/j.conbuildmat.2017.08.022.

Li, M., Anderson, N., Sneed, L., & Torgashov, E. (2016). Condition assessment of concrete pavements using both ground penetrating radar and stress-wave based techniques. *Journal of Applied Geophysics,135*, 297-308. doi:10.1016/j.jappgeo.2016.10.022

Liu, J., Zollinger, D. G., & Lytton, R. L. (2008). Detection of Delamination in Concrete Pavements Using Ground-Coupled Ground-Penetrating Radar Technique. *Transportation Research Record: Journal of the Transportation Research Board,2087*(1), 68-77. doi:10.3141/2087-08

Maierhofer, C. (2003). Nondestructive Evaluation of Concrete Infrastructure with Ground Penetrating Radar. *Journal of Materials in Civil Engineering,15*, 287-297.

Morcous, G., and Erdogmus, E. (2010). "Accuracy of Ground-Penetrating Radar for Concrete Pavement Thickness Measurement," *ASCE Journal of Performance of Constructed Facilities*, ASCE, 24 (6), November/December 2010.

Moruza, G. M., & Ozyildirim, H. C. (2017). Self-Consolidating Concrete in Virginia Department of Transportation's Bridge Structures. *ACI Materials Journal,114*(1). doi:10.14359/51689480

Ozyildirim, C. (2004). Air-Void Characteristics of Concretes in Different Applications. *Transportation Research Record: Journal of the Transportation Research Board,1893*, 70-74. doi:10.3141/1893-09

Shen, Peiliang, and Zhitian Liu. "Study on the Hydration of Young Concrete Based on Dielectric Property Measurement." Construction and Building Materials, vol. 196, 2019, pp. 354–361., doi:10.1016/j.conbuildmat.2018.11.150

Perrot, A., & Rangeard, D. (2016). Effects of mix design parameters on consolidation behavior of fresh cement-based materials. *Materials and Structures,50*(2), 117. doi:10.1617/s11527-016-0988-0

7 APPENDICES

Attached appendices (65 pages) include the GPR scans and related photos from this project.